Jang *et al.*
Journal of Analytical Science and Technology (2024) 15:5
https://doi.org/10.1186/s40543-024-00419-3

Journal of Analytical Science and Technology

RESEARCH ARTICLE Open Access

Novel plasma-polymerized coating facilitates HeLa cell spheroid formation, exerting necroptosis via β-cyclodextrin-encapsulated resveratrol

Sujeong Jang[1], Namwuk Baek[2], Youngsik Seo[1], Hyuna Lim[2], Donggeun Jung[2] and Heonyong Park[1*]

Abstract

Beta-cyclodextrins (β-CDs) comprise a pore for accommodating resveratrol (Res), thereby boosting its bioavailability. Res-incorporated β -CD (Res/CD) may be cytotoxic against both normal and cancer cells. Herein, we examined whether Res/CD exhibits anticancer activity against tumor spheroids, similar to in vivo tumor mass. To prepare three-dimensional spheroids, 1,1,1,3,5,7,7,7 octamethyl-3,5-bis(trimethylsiloxyl) tetrasiloxane (OMBTSTS) was deposited to the surface of the culture dish via plasma polymerization. We observed that HeLa cells grew as spheroids on the OMBTSTS-deposited surface at 20 W plasma power. Res/CD was delivered to the hypoxic core of the spheroid, inducing necrosis, whereas Res was not. Consistently, 10 μM Res alone was not cytotoxic to two-dimensional HeLa cells grown on a culture dish and three-dimensional spheroids. However, Res/CD promoted the necroptosis of spheroids, which were split into small fragments, ultimately inducing cell spheroid death. Collectively, our data suggest that nontoxic levels of Res/CD were efficiently delivered to the hypoxic core of tumor spheroids, promoting cell death. Therefore, Res/CD can be used as an effective anticancer drug. Moreover, the plasma-polymerized OMBTSTS modification technique provides insights into the efficient formation of spheroids in various cancer cell lines.

Keywords Plasma-polymerized coating, Resveratrol, Cyclodextrin, HeLa cells, Necrosis, Apoptosis

Introduction

Tumor spheroid are three-dimensional (3D) tumor analogs that can be used as an in vivo platform to evaluate drug delivery systems and drug efficacy (Mehta et al. 2012). Monolayered two-dimensional (2D) cell cultures can be easily manipulated, rapidly reach confluence, and are consistent. Nevertheless, 3D spheroids, similar to tumors, are more beneficial for developing new antitumor drugs because 2D-grown cells do not mirror real tumors in terms of tissue architecture and physiological microenvironments, including nutrient and oxygen transport. Over the last three decades, various types of tumor spheroids have been developed and tested as appropriate platforms for screening novel antitumor drugs (Costa et al. 2016). Spheroids can be generated using several techniques, including liquid overlay, hanging drop arrays (Tung et al. 2011), microfluidic self-assembly methods (Wu et al. 2008), and 3D scaffold-based cell cultures using hydrogels (Tibbitt and Anseth 2009). If the size and shape of spheroids can be controlled using presently utilized tools, their biomedical applications can be extensively achieved. To this end, introducing innovative methods beyond those previously established is beneficial.

*Correspondence:
Heonyong Park
heonyong@dankook.ac.kr
[1] Department of Molecular Biology and Institute of Nanosensor and Biotechnology, Dankook University, 119 Dandae-ro, Dongnam-gu, Cheonan-si, Chungnam 31116, South Korea
[2] Department of Physics, Sungkyunkwan University, 2066 Seobu-ro, Jangan-gu, Suwon-si, Gyeonggi-do 16419, Republic of Korea

In the present study, we modified the surface of culture dishes using plasma-enhanced chemical vapor deposition (PECVD) to develop tumor cell spheroids. Previously, we used PECVD to modify polystyrene culture dishes for diverse purposes. For example, polystyrene culture dishes modified by depositing plasma-polymerized 4,7,10-trioxa-1,13-tridecanediamine (ppTTDDA) were used to proliferate adipose-derived mesenchymal stem cells (ASC) (Lim et al. 2022). Accordingly, this modification is beneficial for maintaining ASC stemness. Another study demonstrated that ppTTDDA-modified dishes provide an appropriate surface for proliferating and migrating bovine aortic endothelial cells (BAEC) (Lim et al. 2020). Collectively, plasma surface modifications can be applied to provide a surface with the desired properties, thereby increasing surface biocompatibility such that cells can adhere, grow, differentiate, and aggregate into tumor mass-like spheroids. In particular, to generate tumor spheroids, PECVD-based surface modifications may effectively overcome potential hurdles such as laborious and expensive procedures as well as intricate technical complexities.

Resveratrol (Res) is a natural polyphenol with various pharmaceutical functions, including antioxidant, anti-inflammatory, and proapoptotic activities. Despite its wide spectrum of pharmaceutical activities, Res has limited biomedical applications because of its low water solubility. Over the last 20 decades, various attempts have been made to improve the bioapplicability of Res (Smoliga and Blanchard 2014). Notably, the incorporation of Res with cyclodextrins (CDs), a commonly used delivery system, can increase its bioapplications and water solubility (Zhang et al. 2019). The hydrophobic inner cavity of CDs can harbor nonpolar and size-fit polyphenols such as Res. Furthermore, the delivery capability of CDs originates from their chemical properties. CDs comprise several glucopyranoses linked by α-(1,4)-glycosidic bonds (Mehta et al. 2012; Costa et al. 2016). Among the various CDs, β-CD comprises six glucose molecules that form a cyclic structure. The formation of β-CD complexes with diverse hydrophobic guest compounds changes their physicochemical properties by increasing their wettability (Mehta et al. 2012). Therefore, β-CD can be a target for increasing the bioavailability by molecularly encapsulating Res.

In this study, we generated tumor cell spheroids on the surface of PECVD-modified culture dishes and investigated the environmental conditions for generating tumor spheroids. Moreover, we compared the pharmaceutical efficacies of Res and Res-incorporated CD (Res/CD) on 2D monolayered cells and 3D spheroids. Our study findings provide insights into an efficient in vivo-like in vitro screening system for drug development.

Results

Pharmaceutical efficacy of Res in a vehicle is superior to that of Res/β-CD in monolayered cultured cells

First, we measured the viability of Res and Res/CD at various concentrations. Figure 1A illustrates that at 100 μM, both Res and Res/CD exhibited a cytotoxic effect of approximately 47% and 40%, respectively, against BAECs; in contrast, both exhibited no cytotoxic activity at ≤ 10 μM. In the time-course experiments, the cytotoxic activity against 3T3-L1, U937, and HeLa cells increased with an increase in incubation time (Fig. 1B). The cytotoxicity of Res was the highest in HeLa cells (~ 73%) (Fig. 1C). We reanalyzed our data by plotting the cytotoxicity ratio (R) of Res to that of Res/CD against the cytotoxicity of Res (CR). This approach allowed a direct comparison of the cytotoxicity of Res with that of Res/CD. Remarkably, the R of Res compared with that of Res/CD increased as CR increased, following the equation ($R = 2.3 \times CR + 0.6$) (Fig. 1D). This relationship clearly suggests that Res dissolved in ethanol exhibits significantly higher cytotoxicity than Res/CD when applied to cells cultured on commercially available dishes (Fig. 1D). These findings suggest that carrier-dissolved Res is pharmacologically more effective than Res/CD, particularly when treating monolayer-cultured cells in culture dishes.

PECVD modifies the surface of culture dishes, generating 3D HeLa cell spheroids

Although Res is pharmaceutically more efficient than Res/CD in monolayered (2D) cultured cells, whether this result is reproducible in real tumors or 3D spheroids remains unclear. To confirm the reproducibility of Res or Res/CD on 3D spheroids, we first attempted to generate 3D spheroids of HeLa cells, which were the most responsible for Res among the various cells examined (Fig. 1C). We previously reported that PECVD-based surface modification controls cell adhesion and growth (Lim et al. 2020; Kim et al. 2010; Choi et al. 2011; Kwon et al. 2018a; Kwon et al. 2018b). Notably, a non-adhesive surface generates cell aggregates that are the preforms of spheroids (Tung et al. 2011). Based on these reports, we used decamethylcyclopentasiloxane (DMCPS), tris(trimethylsiloxy)silane (TMSS), and 1,1,1,3,5,7,7,7-octamethyl-3,5-bis(trimethylsiloxy)tetrasiloxane (OMBTSTS) as the vaporized chemicals for PECVD. The carrier gas flow rate was varied from 60 to 90 SCCM. Among these variable conditions, PECVD using OMBTSTS as the monomer at 60 SCCM was optimized for 3D spheroid formation (Table 1). Furthermore, we observed that the plasma-polymerized films of OMBTSTS (ppOMBTSTS) were deposited on the surface of the culture dishes (Fig. 2A–D).

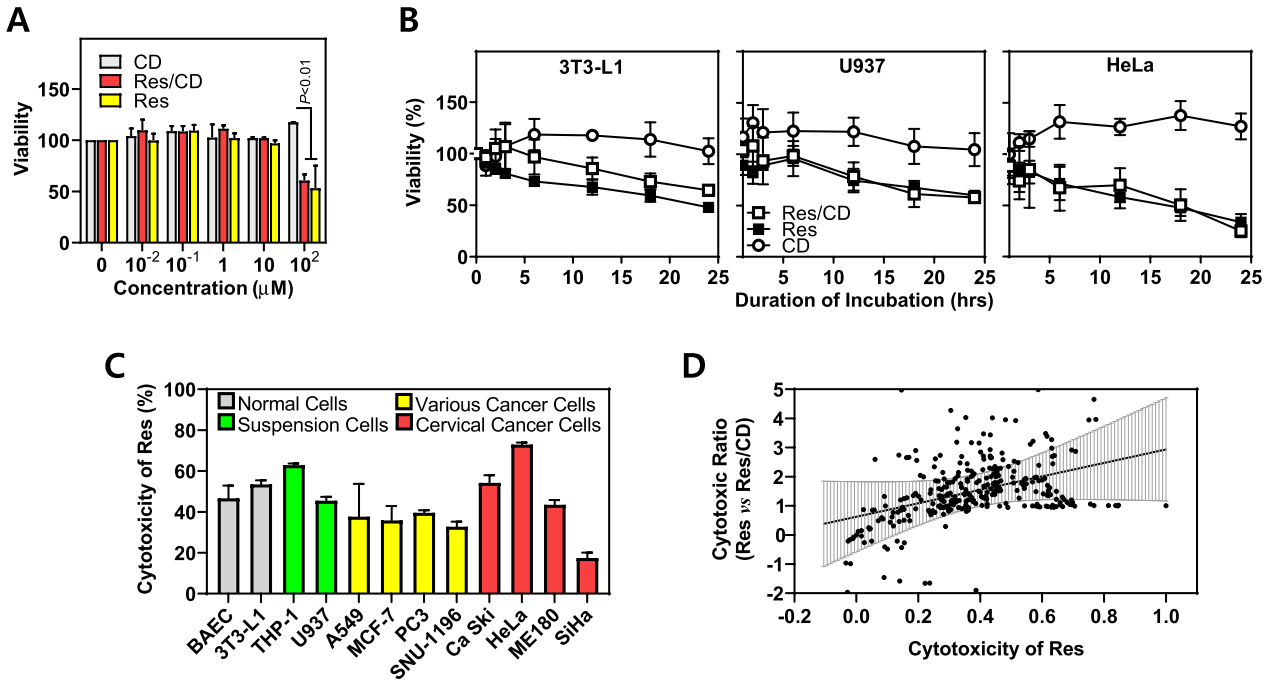

Fig. 1 Resveratrol (Res) alone exerts greater cytotoxic activity on two-dimensional monolayered cells than β-cyclodextrin-encapsulated resveratrol (Res/CD). **A** Bovine aortic endothelial cells (BAECs) were treated with various concentrations of CD, Res, or Res/CD for 24 h. Subsequently, they were stained with WST-1 for 1 h, as suggested by the provider. Then, live cells were monitored based on the OD at 450 nm. The bar graphs represent the percentage of live cells (mean ± SE, n = 3). *p*-values were obtained using one-way analysis of variance and Turkey's test. **B** 3T3-L1, U937, and HeLa cells were treated with 100 μM CD, Res, or Res/CD for up to 24 h. Then, cell viability was measured as previously described in panel A. The line graphs illustrate the percentages of live cells compared with the total cell population (mean ± SE, n = 3). **C** Res cytotoxicity was evaluated using the following formula: [1 − (OD_{450nm} for Res-treated cells/OD_{450nm} for CD-treated cells)] × 100. **D** Relative cytotoxicity of Res compared with that of Res/CD was assessed and plotted against the cytotoxicity of Res in different cell types and under different conditions

Table 1 Cell growth result table by precursor type

No	Monomer	Carrier gas flow rate (SCCM)	Process pressure (Pa)	Process plasma power (W)	Process time (min)	Cellular growth	
						Monolayered cells	Spheroids (numbers/field)
1	DMCPS	60	73	20	10	None	None
2	TMSS	60	73	20	10	Proliferated	2.0
3	TMSS	90	73	20	10	Proliferated	2.1
4	OMBTSTS	60	73	20	10	Minimally	2.9
5	OMBTSTS	90	73	20	10	Minimally	None

A Fig. 2A demonstrates the Water contact angle (WCA) of the treated surfaces. The untreated polystyrene substrate exhibited a WCA of 42.7°; this value is generally associated with oxygen plasma treatment and is commonly used to enhance the adhesion of monolayered (2D) cells to polystyrene substrates [refer to substrate manufacturer's process]. However, after plasma surface modification using the OMBTSTS precursor, the WCA increased to > 99°, indicating a substantial improvement in surface hydrophobicity.

A Fig. 2B shows the C–C–O–C–C stretch bending (1232 cm^{-1}) and aromatic CH_2 bending (680–860 cm^{-1}) peaks in the Fourier transform infrared (FTIR) spectrum of the polystyrene substrate. On the other hand, after plasma surface modification of the polystyrene substrate, the Si–O–Si (950–1150 cm^{-1}) and Si-Me_X $_{(X = 1,2,3)}$ (720–890 cm^{-1}) peaks were observed. In

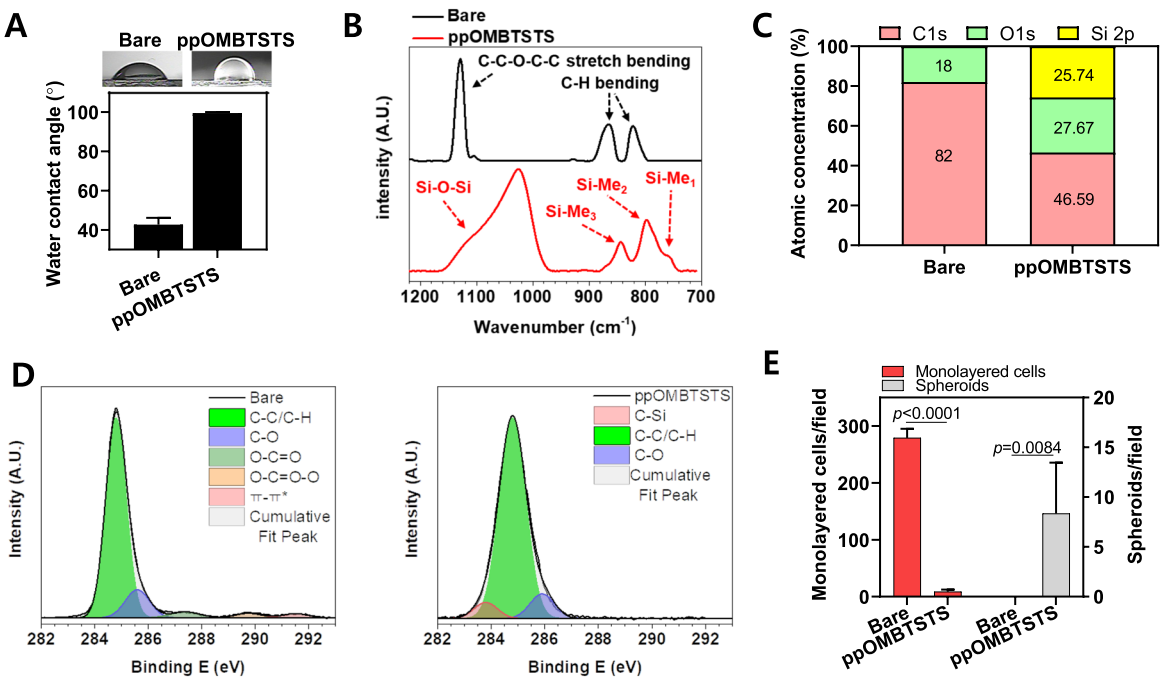

Fig. 2 Characterization of the ppOMBTSTS surface coated on the culture dish for generating HeLa cell spheroids. **A** Water contact angle of polystyrene Petri dishes and ppOMBTSTS surface. The water contact angle data were plotted as bar graphs (n = 2). **B** FT-IR absorption spectra of polystyrene Petri dishes (Bare) and ppOMBTSTS. **C** XPS atomic concentration of polystyrene Petri dishes (Bare) and ppOMBTSTS. **D** Deconvoluted XPS C1s peak of polystyrene Petri dishes (Bare) and ppOMBTSTS for C–Si, C–C/C–H, C–O, O–C=O, O–C=O–O and π–π* peaks. **E** HeLa cells were added to polystyrene Petri dishes (Bare) or ppOMBTSTS surface and incubated for 3 days. Both spheroids and monolayered cells were observed under a microscope. The bar graphs represent the number of spheroids or monolayered cells per visual field (mean ± SE, n = 5)

particular, the Si-$Me_{X\ (X\ =\ 1,2,3)}$ bond has a low surface energy and decreases surface adhesion; therefore, it is widely used as an antifouling coating material (Levasseur et al. 2012).

X-ray photoelectron spectroscopy (XPS) findings are illustrated in Fig. 2C. Plasma surface modification resulted in substantial changes in the types and proportions of the constituent atoms. The substrate (polystyrene) used in this experiment was subjected to oxygen plasma treatment for sterilization and disinfection (Bol'shakov et al. 2004). Oxygen atoms were detected in addition to the typical carbon atoms found in regular polystyrene. The lower oxygen-to-carbon ratio of 18% compared with that of carbon (82%) is attributed to the conventional oxygen plasma treatment primarily occurring at the uppermost surface layers. Because plasma surface modification was performed, the detection of Si was different from the results for bare-surface XPS. This Si originated from the OMBTSTS precursor, indicating the success of plasma surface modification using the OMBTSTS precursor.

The left panel of Fig. 2D demonstrates the results of XPS C1s high-resolution peak deconvolution before and after plasma surface modification of the polystyrene substrate. Deconvolution was performed by correcting the C–C/C–H peak to 284.79 eV using the OriginPro program. In the case of polystyrene substrate, not only the C–C/C–H (284.79 eV) and π–π* (291.01 eV) peaks originating from the backbone structure but also the C–O (285.6 eV) and O–C=O (287.4 eV), O–C=O–O (289.75 eV) peaks can be confirmed (Ba et al. 2016; Browne et al. 2004). However, after plasma surface modification of the PS substrate, the peak originating from the backbone structure of the polystyrene substrate disappeared; in particular, the Si–C (283.79 eV) peak originating from the OMBTSTS precursor structure appeared (Avila et al. 2001). This result is consistent with previous FTIR analysis results. This suggests that 3D cells can be effectively generated by forming Si-Me groups on the surface by appropriately selecting the plasma power (Fig. 2E).

Collectively, the ppOMBTSTS surface serves as the underlying substrate for effectively initiating the growth of HeLa cell spheroids, significantly decreasing monolayered (2D) adherent cells, and generating 3D spheroids (Fig. 2E).

Spheroids grow up to ~ 400 μM within 10 days after inoculating on the ppOMBTSTS-deposited plasma-polymerized film

We counted the spheroids grown on Matrigel and compared them with those generated on the ppOMBTSTS surface (Fig. 3A). The number of spheroids developed on the ppOMBTSTS film was fivefold higher than that developed on Matrigel. Furthermore, the diameter of the spheroids generated on the ppOMBTSTS film appeared to continuously increase until the 7th day after inoculation (Fig. 3B). Larger spheroids (with diameters > 351 μm) reached their maximum distribution 7 days after inoculation (Fig. 3C).

Enhanced detrimental effects of Res/CD on HeLa cell spheroids compared with Res alone

Res at concentrations above 50 μM induces the tumor cell death (Ratajczak and Borska 2021; Yang et al. 2014; Ding and Adrian 2002; Cui et al. 2010). To determine whether the cytotoxic effects of Res extend to 3D spheroids, we systematically elucidated the effects of varying concentrations of Res or Res/CD on HeLa cell spheroids. Treatment with either Res or Res/CD at 50 μM decreased the diameter of the spheroids generated on the ppOMBTSTS surface (Fig. 4A). However, the number of spheroids increased. This suggests that both Res and Res/CD contribute to the fragmentation of spheroids into smaller entities. Nevertheless, at 10 μM, contrasting outcomes were observed for Res and Res/CD: Res exhibited no discernible effect on the spheroids, whereas Res/CD decreased the diameter of the spheroids. In the time-course experiments, 10 μM Res/CD significantly decreased spheroid diameter starting from 48 h compared with 10 μM Res (Fig. 4B). These findings suggest that in terms of bioavailability, Res/CD is more effective against 3D spheroids than Res alone.

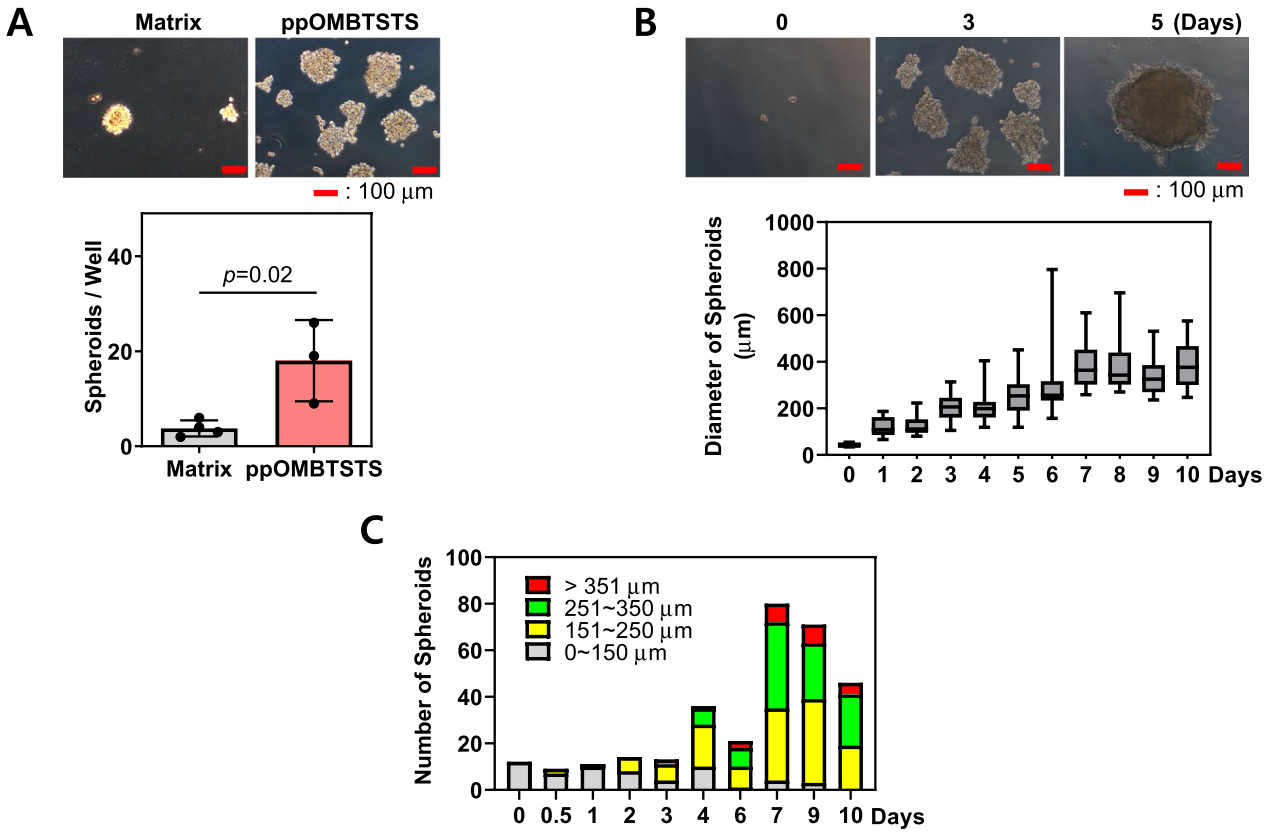

Fig. 3 Development and size distribution analysis of HeLa cell spheroids on ppOMBTSTS surface. **A** Three thousand HeLa cells were added to Matrigel (provided by BME) or a PECVD-coated plate and further incubated for 5 days. Spheroids developed in two different conditions were observed under a microscope. Representative images are displayed in the top panel and the spheroid count was plotted as bar graphs (mean ± SE, n = 3). *p*-values were calculated using Student's t-test. **B** HeLa cell spheroids were grown on PECVD-coated plates for 10 days. Spheroids were observed daily under a microscope, and random images were captured. Subsequently, the count and diameters of the spheroids were measured. Representative images are presented in the top panel. Spheroid diameters were plotted against incubation days (mean ± SE, n = 8–15). **C** Size distributions of HeLa cell spheroids, developed as described in panel B, were replotted against incubation periods

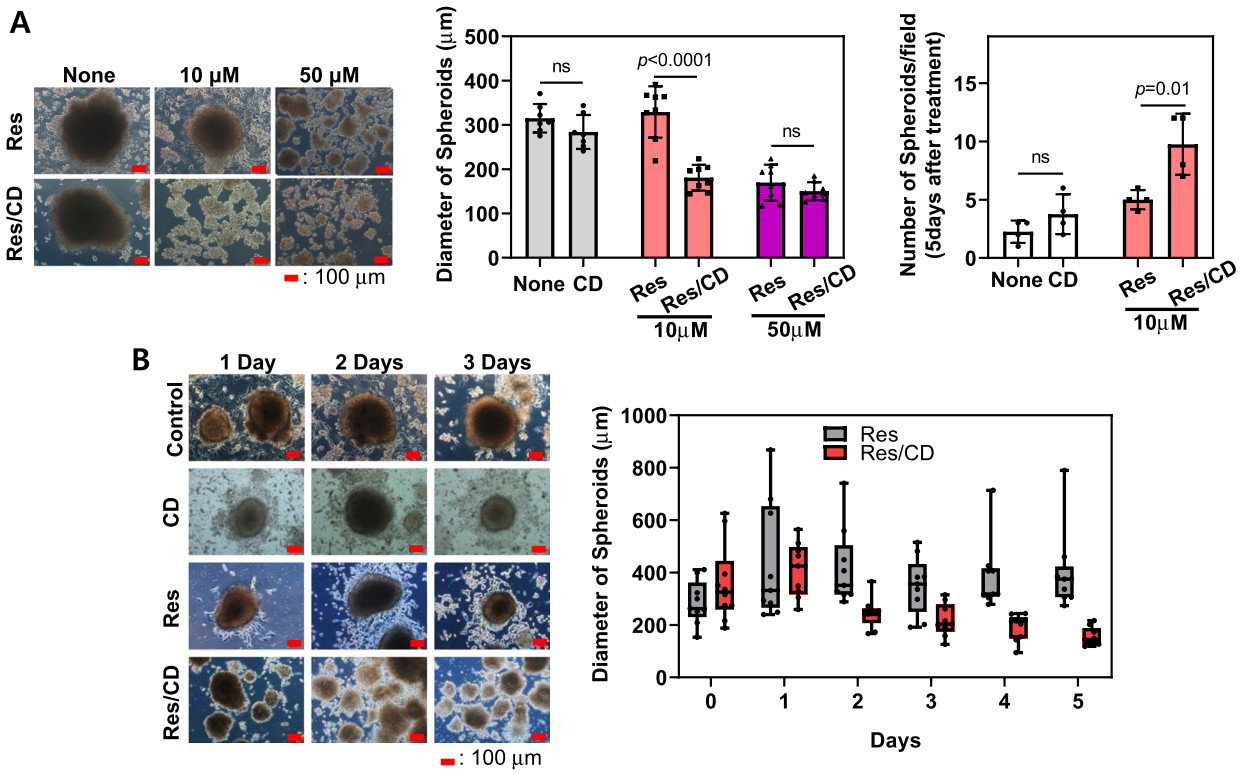

Fig. 4 β-Cyclodextrin-encapsulated resveratrol (Res/CD) exhibits enhanced detrimental effects on HeLa cell spheroids compared with resveratrol (Res) alone. **A** HeLa cell spheroids were generated on the PECVD-coated plate for 5 days as described in Fig. 3 and then treated with 10 or 50 μM of Res or Res/CD for additional 3 days. The bar graphs represent the diameter (in the middle panel) and count of the spheroids (in the right panel). (mean ± SE, n = 8). *p*-values were calculated using the Student's t-test. **B** HeLa cell spheroids were treated as described in panel A. Spheroids or detrimental spheroids were monitored daily under a microscope. Representative images are presented in the left panel, and the data were plotted as bar graphs (mean ± SE, n = 9). *p*-values were < 0.05 using two-way analysis of variance, followed by Tukey's test

CD encapsulation facilitates Res delivery into the necrotic core of spheroids, thereby promoting tumor necrosis

Because of their 3D cultivation, spheroids comprise an outer zone, known as the proliferation zone, and an internal necrotic core (Mehta et al. 2012). The proliferation zone, located at the periphery, directly interacts with nutrient- and oxygen-rich media, whereas the necrotic core experiences oxygen deficiency (hypoxia) and nutrient deprivation. Accordingly, spheroid staining using calcein AM, a live cell marker, and propidium iodide (PI), a necrotic marker, revealed that the outer shells were stained with calcein AM, indicating the presence of live cells; in contrast, the inner core was stained with PI, indicating necrosis (Fig. 5A). The growth conditions of the cells cultivated in a monolayered 2D culture resembled those of the proliferation zone. Nevertheless, conventional 2D cell cultures in nutrient-rich culture dishes do not accurately represent the cells in the necrotic core. Therefore, to replicate the conditions of the necrotic core of spheroids, HeLa cells were subjected to $CoCl_2$ treatment while cultured on a dish to induce necrosis (Bae et al. 2012). When HeLa cells were treated with 0–500 μM $CoCl_2$ for 24 h, HIF-1α expression markedly increased by 4–12-fold at 200–500 μM, indicating that necrosis occurs after treatment with ≥ 200 μM $CoCl_2$ (Fig. 5B). Flow cytometry revealed that $CoCl_2$ alone induces necrosis (Fig. 5C). This finding suggests that hypoxia triggers necrosis in HeLa cells. Res synergistically enhanced $CoCl_2$-induced necrosis by 150% in 2D cells (Fig. 5D). Collectively, our findings suggest that the Res delivered by Res/CD markedly expedites necrosis in the necrotic core of spheroids.

Res/CD promotes the apoptosis of HeLa cell spheroids

We investigated whether Res or Res/CD induces the apoptosis of HeLa cell spheroids. Annexin V flip-flop and nuclear fragmentation confirmed Res-induced apoptosis of the monolayered 2D cells, as monitored by flow cytometry and fluorescence microscopy, respectively (Fig. 6A and B). Flow cytometric analysis revealed that cotreatment with Res (10 μM) and $CoCl_2$ (300 μM) increased apoptosis by four-fold compared with $CoCl_2$

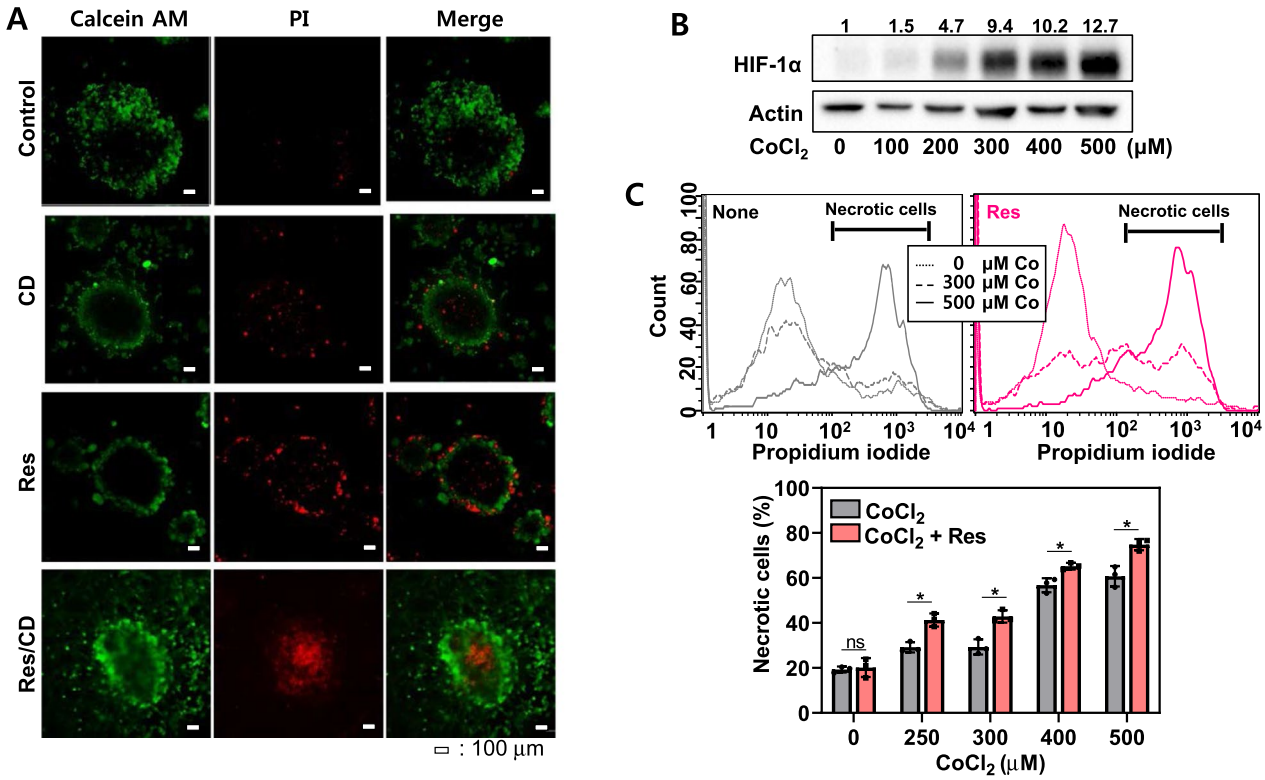

Fig. 5 β-Cyclodextrin-encapsulated resveratrol (CD/Res) significantly enhances necrosis in the hypoxic inner core of HeLa cell spheroids. **A** HeLa cell spheroids were treated with 10 μM β-cyclodextrin (CD), resveratrol (Res), or Res/CD) and then stained with calcein AM and propidium iodide (PI). Stained spheroids were observed under a fluorescence microscope. Representative images are presented in this panel. **B** HeLa cells were treated with 0–500 μM cobalt chloride ($CoCl_2$) for up to 24 h, followed by immunoblotting of cell lysates with anti-HIF-1α antibody. Densitometry was used to quantify HIF-1α levels. **C** HeLa cells were treated with 0–500 μM $CoCl_2$ with or without 10 μM Res and then stained with PI. PI-stained cells were analyzed via flow cytometry. **D** The bar graphs depict the quantity of necrotic HeLa cells (mean ± SE, n = 3). *$p < 0.05$ (two-way analysis of variance and Turkey's test). ns = not significant

treatment alone (Fig. 6A). We observed that when the spheroids were exposed to 10 μM Res or Res/CD, caspase-3 was activated by Res/CD but not by Res alone (Fig. 6C). Consistently, as shown in Fig. 6D, 10 μM Res activated caspase-3 in $CoCl_2$-preconditioned cells; in contrast, Res did not affect 2D unconditioned cells. These findings suggest that low-dose Res (~ 10 μM) triggers the apoptosis of hypoxic cells, such as those in the necrotic core. Notably, low-dose Res is not cytotoxic to normal cells (In et al. 2006).

Discussion

Accumulating evidence suggests that Res exerts various biological activities, including anti-inflammatory, anticancer (In et al. 2006; Cai et al. 2015; de Sa Coutinho et al. 2018; Rauf et al. 2018; Varoni et al. 2016), and antifungal activities (Gabaston et al. 2017). Despite its wide range of pharmaceutical activities, Res has limited biomedical applications because of its poor water solubility and low bioavailability. Nevertheless, many studies have revealed the beneficial effects of Res via in vitro experiments; however, these findings are not always consistent with those of in vivo studies. This disparity stems from delivery challenges, which are primarily associated with the poor water solubility of lipophilic drugs, including Res. In the present study, CDs were used to address this issue. CDs are synthesized from several glucopyranoses, generating a cyclic truncated cone-like structure with a hydrophilic outer surface and a lipophilic inner cavity (Kfoury et al. 2018; Armstrong et al. 1986). The three distinct CDs, namely α-, β-, and γ-CDs, comprise six, seven, and eight glucopyranose units, respectively. α-, β-, and γ-CDs exhibit average inner and outer cavity diameters of 0.57/1.37 nm, 0.78/1.53 nm, and 0.95/1.69 nm, respectively (Jeandet et al. 2021). A previous study has revealed that the pore size of α-CDs is extremely small for Res internalization, thereby exhibiting the lowest binding affinity among the three CDs (Haley et al. 2020). Furthermore, although the binding affinities of β-CD and γ-CD are comparable (−5.4 kcal/mol and −5.3 kcal/mol respectively), the loading yield of Res in β-CD surpasses that in γ-CD by 1.5-fold, as reported previously (Haley

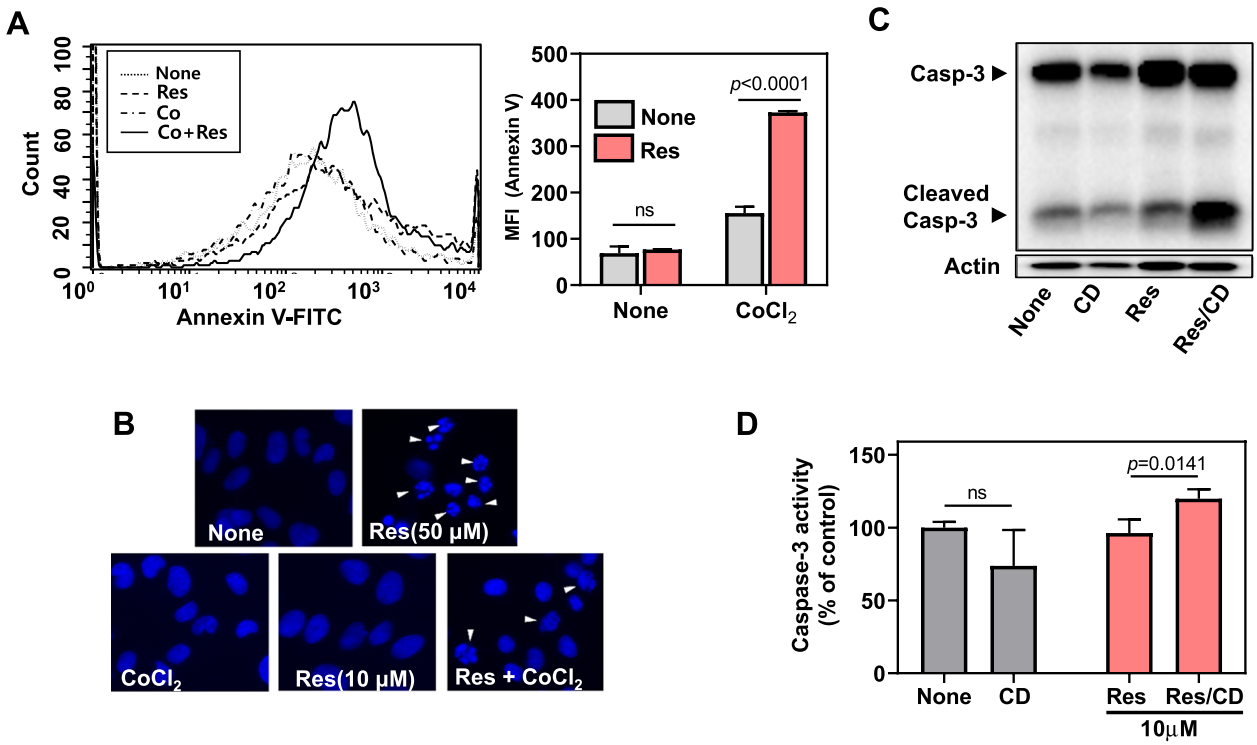

Fig. 6 β-Cyclodextrin-encapsulated resveratrol (Res/CD) induces apoptosis in the hypoxic inner core of HeLa cell spheroids. **A** HeLa cells grown till confluence were treated with 300 μM $CoCl_2$ and/or 10 μM resveratrol (Res) for 24 h and then stained with annexin-V-FITC. Thereafter, annexin-V-FITC-stained cells were analyzed via flow cytometry. The bar graphs represent the number of apoptotic HeLa cells (mean ± SE, n = 3). *p*-values were calculated using Student's t-test. **B** HeLa cells were treated with 300 μM $CoCl_2$ and/or 10 μM Res for 24 h and stained with 4′, 6-diamidino-2-phenylindole. Fragmented nuclei (indicated using white arrowheads) were observed under a fluorescence microscope. **C** HeLa spheroid cells were lysed and immunoblotted with an anti-caspase-3 antibody. The levels of cleaved caspase-3 were quantified using densitometry. **D** To measure caspase-3 activity, HeLa cell spheroids were treated with various reagents mentioned in the Materials and Methods sections. FITC fluorescent intensity (excitation wavelength: 485 nm, emission wavelength: 525 nm) indicates caspase-3 activity. The bar graphs depict caspase-3 activity (mean ± SE, n = 3 ~ 6). *p*-values were calculated using Student's t-test. ns = not significant

et al. 2020). Therefore, in this study, we used β-CD to internalize Res.

Next, to improve the solubility of β-CD, chemically modified β-CDs have been used to internalize lipophilic drugs (Park et al. 1998; Bonnet et al. 2015; Gidwani and Vyas 2015; Lucas-Abellán et al. 2007; Pinho et al. 2014; Stella and Rajewski 2020; Sandilya et al. 2020). Although improving its solubility, modified β-CD often exhibits increased toxicity, for example, the disintegration of lipid rafts and cholesterol efflux (Park et al. 1998). In contrast, in our previous study, we reported that unmodified β-cyclodextrin remains noncytotoxic even at concentrations as high as 800 μg/ml (Jang et al. 2020). Accordingly, unmodified β-CD can serve as a drug carrier owing to its nontoxic nature.

Based on its concentrations, Res exhibits bifurcated functions: bioactive functions at low doses (< 10 μM) and antiproliferative or proapoptotic activities at high doses (> 20 μM). The biological activities exerted by Res in vitro are diverse, including inflammation regulation (Donnelly et al. 2004), neuroprotective activities (Velmurugan et al. 2018), and cardiovascular function regulation (Seo et al. 2019; Dyck et al. 2019). However, its antitumor or proapoptotic activities have been confirmed in various cancer cell lines, including pancreatic, stomach, and liver cancers (Ratajczak and Borska 2021). In addition, the chemotherapeutic dose of Res is approximately 40 μM for cervical cancer, as observed in HeLa cells (Sun et al. 2020). Therefore, the issue concerning Res bioavailability in cancer treatment revolves around the challenge of administering high therapeutic doses, which can negatively affect normal cells. Interestingly, in the present study, we demonstrated that the death of HeLa cell spheroids was initiated at a low dose (10 μM), which does not harm normal cells. The efficacy observed at a low dose can be attributed to the hypoxic microenvironment in the necrotic core, a phenomenon that occurs in spheroids but not in 2D cell cultures. This hypothesis is supported by our results, which indicate that Res induces significantly higher necrosis and apoptosis levels in cells

exposed to $CoCl_2$-induced hypoxia (see Figs. 5 and 6). Our study findings demonstrate the efficient delivery of Res to the necrotic core by Res/CD; however, Res alone does not exhibit the same capability (Figs. 5 and 6). This phenomenon cannot be easily explained because Res/CD is larger than Res. However, this observation may be explained by the hypothesis that the surface of Res/CD is more hydrophilic than that of Res, potentially facilitating access to the inner necrotic core.

We used three compounds (DMCPS, TMSS, and OMBTSTS) for spheroid formation. All three compounds contain Si–O–Si and CH_3 groups. Table 1 summarizes that OMBTSTS is an optimal monomer for enhancing surface construction, resulting in improved spheroid formation and the decreased proliferation of monolayered (2D) cells. XPS revealed that the ratio of O1s (27.67%) was higher and that of Si2p (25.74%) was lower in OMBTSTS than in TMSS (23% of O1s and 29% of Si2p) (Fig. 2C and Additional file 1: Fig. S1). These findings suggest that the percentage increase in O1s and percentage decrease in Si2p are positively correlated with spheroid formation promotion. Moreover, FTIR data revealed that the ppOMBTSTS surface contains a higher proportion of dimethylsilyl groups and a lower proportion of trimethylsilyl groups than the ppTMSS surface (Additional file 1: Fig. S1B), suggesting that increased methylation is not conducive to spheroid formation. The differential alterations observed between the surfaces coated using OMBTSTS and TMSS can be attributed to minor modifications of the monomer during PECVD. In addition, when comparing the space-filling models of DMCPS, TMSS, and OMBTSTS, the shielding effect of the Si–O–Si groups by CH_3 groups is more pronounced in OMBTSTS (Additional file 1: Fig. S2), possibly facilitating the development of an appropriate surface for generating 3D spheroids after PECVD. Moreover, our data revealed that a lower carrier flow rate was more conducive to spheroid generation than a higher flow rate (60 vs. 90 SCCM) (Table 1). The plasma power used in this study was 20 W, which is relatively lower than that used in other conventional PECVD methods (Gölander et al. 1993). Enhanced 3D spheroid formation at a low plasma power suggests that preserving the intact structure of the monomer is vital for spheroid cultivation. Therefore, the intact structure of OMBTSTS deposited on the surface may provide a more favorable microenvironment for spheroid growth than that of DMCPS and TMSS. However, the detailed underlying molecular mechanisms remain unelucidated.

The average diameter of spheroids produced in this study was approximately 380 μm; this is similar to the diameters of spheroids generated using alternative methods. Notably, larger spheroids (approximately 400 μm in diameter) exhibit distinct regions, including an inner necrotic core, a middle quiescent zone, and an outer proliferation zone. However, the spheroids developed in this study lacked an inner necrotic core. This observation is supported by the results illustrated in Fig. 5A, where spheroids were negative for PI staining, which indicates necrotic cores. Nevertheless, the slight increase in PI staining observed in the spheroids (Fig. 5A) suggests the emergence of hypoxic conditions within the inner core of the spheroids engineered in this study. In the presence of hypoxia in these spheroids, Res administration via the Res/CD approach induces cell death in the inner core. At present, the efficacy of Res/CD in larger spheroids (with diameters exceeding 400 μm) that harbor a necrotic core remains unelucidated. In summary, our findings provide valuable insights into the pharmaceutical applications of Res/CD, particularly highlighting its enhanced efficacy in developing tumors (~ 380 μm in diameter) exposed to hypoxic conditions.

Conclusions

In this study, we confirmed that the efficacy of drugs on 3D spheroids differs significantly from that observed in 2D cell culture. Therefore, the construction of 3D spheroids is a prerequisite for evaluating the in vitro antitumoric activity of a drug, specifically Res. We found that the surface modification using ppOMBTSTS offers an exceptional option for establishing a platform conducive to the construction of 3D spheroids. Furthermore, this study reveals that non-toxic concentrations of Res/CD selectively induce necroptosis in tumor spheroids, as opposed to 2D cancer cells (see Fig. 7).

Materials and methods

Cell culture, reagents, and treatments

HeLa, MCF-7, and SNU-1196 cells were cultured in Dulbecco's modified Eagle's medium (DMEM, Welgene Inc. Gyeongsan, Korea) supplemented with 20% fetal bovine serum (FBS, Welgene Inc.) and antibiotics (penicillin and streptomycin). 3T3-L1 cells were cultured in DMEM supplemented with 10% bovine calf serum (Welgene Inc.) and antibiotics (penicillin and streptomycin). A549, PC3, THP-1, U937, Ca Ski, and ME180 cells were cultured in Roswell Park Memorial Institute medium (Welgene Inc.) supplemented with 10% FBS and antibiotics (penicillin and streptomycin). BAECs were derived from the descending thoracic aorta and cultured in DMEM supplemented with 20% FBS and antibiotics (penicillin and streptomycin). All cells were grown in a humidified incubator in a 5% CO_2 atmosphere at 37 °C. To assess cell viability, cells were treated with 0–100 μM Res (Sigma-Aldrich, St. Louis, MO, USA) or Res/CD and cobalt chloride ($CoCl_2$, Sigma-Aldrich) for 24 h.

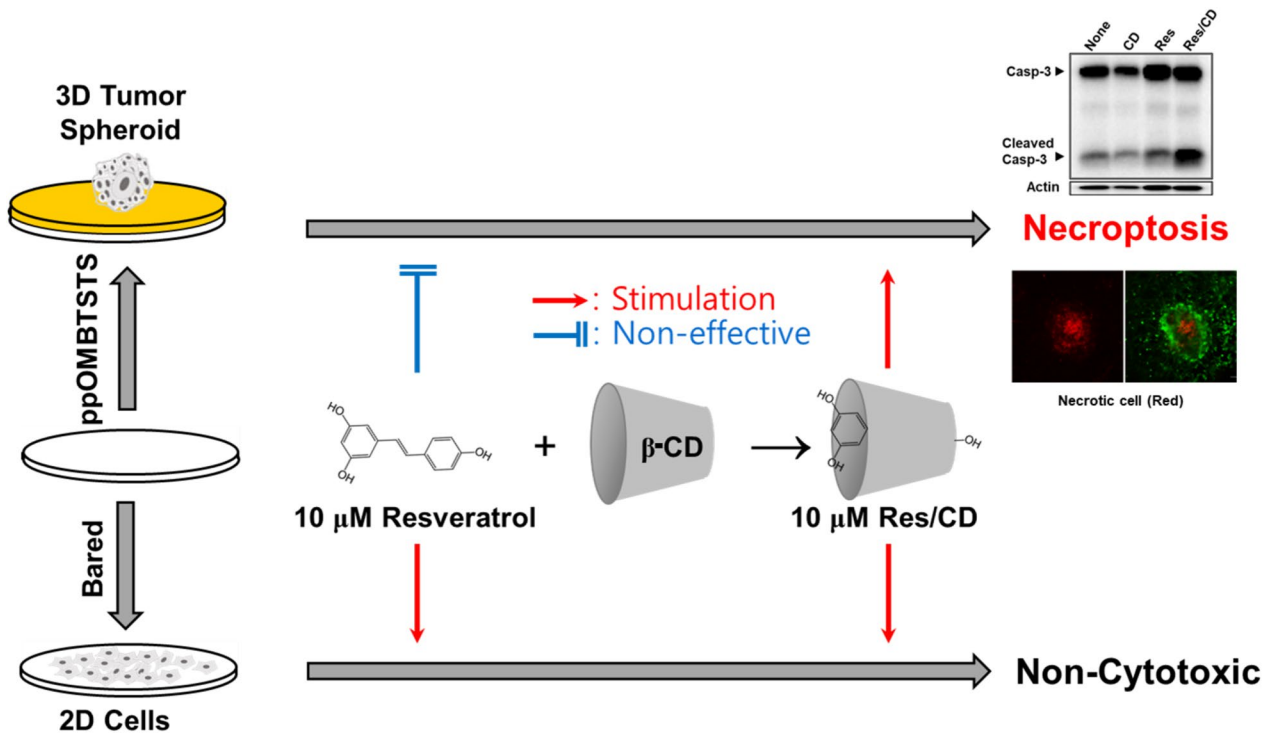

Fig. 7 Schematic diagram depicting an anti-tumoric activity of Res/CD on 3D spheroids constructed using ppOBMTSTS

Viability test

Cells were grown in appropriate media on 96-well culture dishes. After reaching confluency and serum starvation for 2 h, cells were treated with tetrazolium salt (WST-1, Daeil Lab Service Co., Seoul, Korea) for 2 h according to the manufacturer's instructions. To monitor the effect of CD, Res, or Res/CD on cell viability, cells were pretreated with various concentrations of CD, Res, or Res/CD for 0–24 h and subsequently exposed to WST-1. Finally, WST-1-produced formazan in live cells was measured at 450 nm using a spectrophotometer (Epoch, Agilent, CA, USA).

Surface modification of polystyrene Petri dishes via plasma polymerization

Plasma modification experiments were conducted using the precursor octamethyl-3,5-bis(trimethylsiloxy) tetrasiloxane (OMBTSTS) in a PECVD system. This precursor was selected because of its distinct structure and potential for plasma modification applications. Surface modification was conducted at a plasma power of 20 W to preserve the characteristics of the precursor (Yasuda et al. 1976) because a plasma power of < 20 W does not provide sufficient energy to maintain the plasma state. On the other hand, when the plasma power is > 20 W, dissociation in the precursor structure increases (Gölander et al. 1993), thereby decreasing the characteristics of the precursor structure and causing substrate damage (Fukasawa et al. 2011) because of increased ion bombardment energy. This finding indicates the importance of maintaining the plasma power within a specified range to avoid adverse effects.

Water contact angle measurement

The fixed-drop method (FM40 Easy Drop; KRUS GmbH, Germany) was used to measure WCA. Deionized water (0.5 μl) was dropped onto the surface of the samples. Immediately, an image of the water that formed on the surface was captured using an adjacent camera. Open-source ImageJ software was used to determine the contact angle. Five measurements were performed for each sample.

Fourier transform infrared spectroscopy measurements

FTIR spectroscopy (Vertex 70, Bruker, USA) was performed using the attenuated total reflectance technique. The vibrational characteristics of the chemical bonds of the investigated materials were examined in the 600–4000 cm^{-1} range, with a resolution of 4 cm^{-1} in the absorbance mode. All measurements were conducted in air and the samples were dried at room temperature.

X-ray photoelectron spectroscopy measurement

A photoelectron spectrometer (AXIS Supra, Kratos, UK) with monochromatic Al Kα X-ray sources at 1486.6 eV was used to perform XPS analysis. All spectra were calibrated by assigning aliphatic carbon at 284.79 eV. High-resolution spectra were deconvoluted using OriginPro software (OriginLab Corp., Northampton, MA, USA) with Shirley background subtraction and Gaussian functions.

Generation of spheroids

HeLa cells were detached from adherent cells grown to confluency using TE (0.25% porcine trypsin and 1 mM EDTA). Then, the suspended cells were counted using a cell counter (LUNA-II™, Logos Biosystems, Anyang, Korea). Three thousand cells were aliquoted into 24-well plates coated with PECVD under various conditions and filled with DMEM supplemented with 10% bovine calf serum. Subsequently, PECVD-coated plates were incubated in a 5% CO_2 humidified incubator at 37 °C for 1–10 days. The spheroids that developed on the dishes were observed under a microscope (Axiovert 40 CFL, ZEISS, Oberkochen, Germany).

Western blotting

A previously described method was used to perform western blotting (Seo et al. 2019). Briefly, HeLa cells or spheroids were lysed with RIPA buffer (150 mM sodium chloride, 1% NP-40, 0.5% deoxycholate, 0.1% sodium dodecyl sulfate [SDS], and 50 mM Tris–HCl) and, if necessary, sonicated using a sonicator (Vibra-Cell VCX 130, Sonics, CT, USA). The total protein content of the cell lysates was measured using a BCA assay kit (Thermo Fisher Scientific, MA, USA). Proteins (25 μg) in the soluble lysates were resolved via 6%–10% SDS–polyacrylamide gel electrophoresis, transferred onto a polyvinylidene difluoride membrane (Millipore, Milford, MA, USA), and blotted with antibodies specific for caspase-3 (Cell Signaling, Danvers, MA, USA) and actin (Santa Cruz Biotechnology, Dallas, USA). Subsequently, the membranes were incubated with horseradish peroxidase-conjugated secondary antibodies and developed using an enhanced chemiluminescence system (Amersham Piscataway, NJ, USA).

Flow cytometry analysis

Monolayered (2D) HeLa cells were grown to confluence, serum-starved for 2 h, and treated with various concentrations of CD or Res and/or $CoCl_2$ for 24 h. Cells exposed to the reagents were detached using TE, washed with phosphate-buffered saline (PBS), and harvested by centrifuging at 800*g* for 3 min. The cells were then washed thoroughly and resuspended in PBS. The cells were stained with annexin V-FITC and PI using the ApoScan™ Annexin V FITC apoptosis detection Kit (Ncbit, Seongnam, Korea) according to the manufacturer's instructions. Briefly, annexin V–FITC was added to the resuspended cells and incubated for 15 min in the dark. To remove unbound annexin V-FITC, the cell suspensions were centrifuged at 1000*g* for 5 min. After removing the supernatant, the precipitated cells were resuspended in a binding buffer. Finally, cells were stained with PI (30 μg/ml) for 10 min. The stained cells were analyzed using a flow cytometer (Guava easyCyte, Millipore).

Fluorescence imaging

Spheroid HeLa cells were stained with calcein AM (1 μM, Cayman Chemical, Michigan, USA) for 1 h and PI (10 μg/ml) for 1 h at room temperature. Spheroids were observed using FITC (excitation wavelength: 485 nm, emission wavelength: 518 nm) and tetramethylrhodamine (excitation wavelength: 547 nm, emission wavelength: 572 nm) filters under a confocal fluorescence microscope (LSM 700, ZEISS). To assess the apoptosis of the spheroids, they were stained with the FITC–DEVD–FMK reagent of the Cleaved Caspase-3 Staining Kit (Abcam) and incubated for 30 min in a 37 °C incubator with a 5% CO_2 atmosphere. The stained spheroid cells were centrifuged at 1000*g* for 5 min, followed by the removal of the supernatant. The precipitated spheroid cells were resuspended in wash buffer. The fluorescence of the stained spheroid cells was measured using a fluorescence reader (Synergy HTX multimode reader, Agilent; excitation wavelength: 485 nm, emission wavelength: 515 nm). To monitor the apoptosis of monolayered (2D) HeLa cells, the cells were fixed with cold 4% paraformaldehyde for 10 min at room temperature. The cells were then mounted with a mounting solution containing 4′, 6-diamidino-2-phenylindole (Vector Laboratories, Inc., Burlingame, CA, USA) and observed under a fluorescence microscope (EVOS M5000, Thermo Fisher Scientific).

Statistical analysis

Data are presented as mean ± SEM and evaluated via analysis of variance (ANOVA) followed by Tukey's post-hoc multiple comparison test. Data were analyzed using GraphPad Prism 8.0 (GraphPad Prism Software Inc., San Diego, CA, USA). Differences were considered statistically significant at a p-value of < 0.05. Student's t-test was used to compare the means between two groups.

Abbreviations

CDs	Cyclodextrins
β-CDs	β-Cyclodextrins
Res	Resveratrol

Res/CD	Res-incorporated β-CD
ppOMBTSTS	Plasma-polymerized films of 1,1,1,3,5,7,7,7 Octamethyl-3,5-bis(trimethylsiloxyl) tetrasiloxane
3D	Three-dimensional
2D	Monolayered two-dimensional
PECVD	Plasma-enhanced chemical vapor deposition
ppTTDDA	Plasma-polymerized 4,7,10-trioxa-1,13-tridecanediamine
ASC	Adipose-derived mesenchymal stem cells
BAEC	Bovine aortic endothelial cell
R	Ratio
CR	Cytotoxicity of Res
DMCPS	Decamethylcyclopentasiloxane
TMSS	Tris(trimethylsiloxy)silane
DMEM	Dulbecco's modified Eagle's medium
FBS	Fetal bovine serum
WCA	Water contact angle
FTIR	Fourier transform infrared
XPS	X-ray photoelectron spectroscopy
PI	Propidium iodide
ANOVA	Analysis of variance

Supplementary Information

The online version contains supplementary material available at https://doi.org/10.1186/s40543-024-00419-3.

Additional file 1: Figure S1. Characterization of ppOMBTSTS and ppTMSS surface coatings. **A** XPS atomic concentration of PS petri dishes (Bare) and ppTMSS. **B** FT-IR absorption spectra of ppOMBTSTS and ppTMSS. **Figure S2.** Space filing models of DMCPS (**A**), TMSS (**B**) and OMBTSTS (**C**). Each distinct color represents a specific atom: hydrogen (white), carbon (gray), silicon (gold), and oxygen (red)

Acknowledgements
None.

Author contributions
SJ contributed to methodology, investigation and data curation. NB contributed to data curation and formal analysis. YS contributed to methodology. HL contributed to formal analysis. DJ contributed to conceptualization. HP contributed to supervision, writing and project administration.

Funding
This study was supported by the Basic Science Research Program of the National Research Foundation of Korea and was funded by the Ministry of Education, Science, and Technology (NRF-2016R1D1A1B02007197 & NRF-2019R1A6A1A10073079).

Availability of data and materials
Data will be made available on reasonable request.

Declarations

Competing interests
None.

Received: 23 January 2024 Accepted: 6 February 2024
Published online: 16 February 2024

References

Armstrong DW, Ward TJ, Armstrong RD, Beesley TE. Separation of drug stereoisomers by the formation of beta-cyclodextrin inclusion complexes. Science. 1986;232(4754):1132–5. https://doi.org/10.1126/science.3704640.
Avila A, Montero I, Galán L, Ripalda JM, Levy R. Behavior of oxygen-doped SiC thin films: an X-ray photoelectron spectroscopy study. J Appl Phys. 2001;89:212–6. https://doi.org/10.1063/1.1332796.
Ba OM, Marmey P, Anselme K, Duncan AC, Ponche A. Surface composition XPS analysis of a plasma treated polystyrene: evolution over long storage periods. Colloids Surf B Biointerfaces. 2016;145:1–7. https://doi.org/10.1016/j.colsurfb.2016.04.026.
Bae S, Jeong HJ, Cha HJ, Kim K, Choi YM, An IS, et al. The hypoxia-mimetic agent cobalt chloride induces cell cycle arrest and alters gene expression in U266 multiple myeloma cells. Int J Mol Med. 2012;30(5):1180–6. https://doi.org/10.3892/ijmm.2012.1115.
Bol'shakov AA, Cruden BA, Mogul R, Rao MVVS, Sharma SP, Khare BN, Meyyappan M. Radio-frequency oxygen plasma as a sterilization source. AIAA J. 2004;42:823–32. https://doi.org/10.2514/1.9562.
Bonnet V, Gervaise C, Djedaini-Pilard F, Furlan A, Sarazin C. Cyclodextrin nanoassemblies: a promising tool for drug delivery. Drug Discov Today. 2015;20(9):1120–6. https://doi.org/10.1016/j.drudis.2015.05.008.
Browne MM, Lubarsky GV, Davidson MR, Bradley RH. Protein adsorption onto polystyrene surfaces studied by XPS and AFM. Surf Sci. 2004;553:155–67. https://doi.org/10.1016/j.susc.2004.01.046.
Cai H, Scott E, Kholghi A, Andreadi C, Rufini A, Karmokar A, et al. Cancer chemoprevention: evidence of a nonlinear dose response for the protective effects of resveratrol in humans and mice. Sci Transl Med. 2015;7(298):298ra117. https://doi.org/10.1126/scitranslmed.aaa7619.
Choi C, Jung D, Moon DW, Lee TG. Surface analysis of protein-resistant, plasma-polymerized ethylene glycol thin films. Surf Interface Anal. 2011;43(3):331–5. https://doi.org/10.1002/sia.3641.
Costa EC, Moreira AF, de Melo-Diogo D, Gaspar VM, Carvalho MP, Correia IJ. 3D tumor spheroids: an overview on the tools and techniques used for their analysis. Biotechnol Adv. 2016;34(8):1427–41. https://doi.org/10.1016/j.biotechadv.2016.11.002.
Cui J, Sun R, Yu Y, Gou S, Zhao G, Wang C. Antiproliferative effect of resveratrol in pancreatic cancer cells. Phytother Res. 2010;24(11):1637–44. https://doi.org/10.1002/ptr.3157.
de Sa Coutinho D, Pacheco MT, Frozza RL, Bernardi A. Anti-inflammatory effects of resveratrol: mechanistic insights. Int J Mol Sci. 2018. https://doi.org/10.3390/ijms19061812.
Ding XZ, Adrian TE. Resveratrol inhibits proliferation and induces apoptosis in human pancreatic cancer cells. Pancreas. 2002;25(4):e71–6. https://doi.org/10.1097/00006676-200211000-00024.
Donnelly LE, Newton R, Kennedy GE, Fenwick PS, Leung RH, Ito K, et al. Anti-inflammatory effects of resveratrol in lung epithelial cells: molecular mechanisms. Am J Physiol Lung Cell Mol Physiol. 2004;287(4):L774–83. https://doi.org/10.1152/ajplung.00110.2004.
Dyck GJB, Raj P, Zieroth S, Dyck JRB, Ezekowitz JA. The effects of resveratrol in patients with cardiovascular disease and heart failure: a narrative review. Int J Mol Sci. 2019. https://doi.org/10.3390/ijms20040904.
Fukasawa M, Nakakubo Y, Matsuda A, Takao Y, Eriguchi K, Ono K, Minami M, Uesawa F, Tatsumi T. Structural and electrical characterization of H/Br O2 plasma damage to plasma substrate. J Vac Sci Technol A. 2011;29:041301. https://doi.org/10.1116/1.3596606.
Gabaston J, Cantos-Villar E, Biais B, Waffo-Teguo P, Renouf E, Corio-Costet MF, et al. Stilbenes from *Vitis vinifera* L. waste: a sustainable tool for controlling *Plasmopara viticola*. J Agric Food Chem. 2017;65(13):2711–8. https://doi.org/10.1021/acs.jafc.7b00241.
Gidwani B, Vyas A. A Comprehensive review on cyclodextrin-based carriers for delivery of chemotherapeutic cytotoxic anticancer drugs. Biomed Res Int. 2015;2015:198268. https://doi.org/10.1155/2015/198268.
Gölander C-G, Rutland MW, Cho DL, Johansson A, Ringblom H, Jönsson S, Yasuda HK. Structure and surface properties of diaminocyclohexane plasma polymer films. J Appl Polym Sci. 1993;49:39–51. https://doi.org/10.1002/app.1993.070490106.
Haley RM, Zuckerman ST, Dakhlallah H, Capadona JR, von Recum HA, Ereifej ES. Resveratrol delivery from implanted cyclodextrin polymers provides sustained antioxidant effect on implanted neural probes. Int J Mol Sci. 2020. https://doi.org/10.3390/ijms21103579.
In K, Park J, Park H. Resveratrol at high doses acts as an apoptotic inducer in endothelial cells. Cancer Res Treat. 2006;38(1):48–53. https://doi.org/10.4143/crt.2006.38.1.48.
Jang S, Lee S, Park H. Beta-cyclodextrin inhibits monocytic adhesion to endothelial cells through nitric oxide-mediated depletion of cell adhesion molecules. Molecules. 2020. https://doi.org/10.3390/molecules25163575.

Jeandet P, Sobarzo-Sanchez E, Uddin MS, Bru R, Clement C, Jacquard C, et al. Resveratrol and cyclodextrins, an easy alliance: applications in nanomedicine, green chemistry and biotechnology. Biotechnol Adv. 2021;53:107844. https://doi.org/10.1016/j.biotechadv.2021.107844.
Kfoury M, Landy D, Fourmentin S. Characterization of cyclodextrin/volatile inclusion complexes: a review. Molecules. 2018. https://doi.org/10.3390/molecules23051204.
Kim KS, Choi C, Kim SH, Choi KO, Kim JM, Kim HJ, Yeo S, Park H, Jung D. Selective adhesion of intestinal epithelial cells on patterned films with amine functionalities formed by plasma enhanced chemical vapor deposition. Appl Surf Sci. 2010;257:398–403. https://doi.org/10.1016/j.apsusc.2010.06.092.
Kwon S, Ban W, Seo Y, Park H, Baik KY, Kim Y, Cho Y, Jung D. Improved adhesion of human umbilical-vein endothelial cells on polystyrene Petri dishes by the formation of functional groups by Ar/H2 plasma modification. J Biomater Tissue Eng. 2018a;8(12):1142–9. https://doi.org/10.1166/jbt.2018.1848.
Kwon S, Ban W, Lim H, Seo Y, Park H, Kim EJ, Cho YK, Park SG, Jung D. Effects of the generated functional groups by PECVD on adhesiveness of adipose-derived mesenchymal stem cells. J Vac Sci Technol A. 2018b;36:031403. https://doi.org/10.1116/1.5020851.
Levasseur O, Stafford L, Gherardi N, Naudé N, Blanchard V, Blanchet P, Riedl B, Sarkissian A. Deposition of hydrophobic functional groups on wood surfaces using atmospheric-pressure dielectric barrier discharge in helium hexamethyldisiloxane gas mixtures. Plasma Process Polym. 2012;9:1168–75. https://doi.org/10.1002/ppap.201100222.
Lim H, Park Y, Seo Y, Park H, Cho YK, Jung D. Surface modification of polystyrene Petri dishes by plasma polymerized 4,7,10-trioxa-1,13-tridecanediamine for enhanced culturing and migration of bovine aortic endothelial cells. Biofouling. 2020;36(7):816–24. https://doi.org/10.1080/08927014.2020.1821878.
Lim H, Park Y, Jang S, Park H, Cho YK, Jung D. Enhanced culturing of adipose derived mesenchymal stem cells on surface modified polystyrene Petri dishes fabricated by plasma enhanced chemical vapor deposition system. J Biomed Mater Res B Appl Biomater. 2022;110(2):358–66. https://doi.org/10.1002/jbm.b.34912.
Lucas-Abellán C, Fortea I, López-Nicolás JM, Núñez-Delicado E. Cyclodextrins as resveratrol carrier system. Food Chem. 2007;104:39–44. https://doi.org/10.1016/j.foodchem.2006.10.068.
Mehta G, Hsiao AY, Ingram M, Luker GD, Takayama S. Opportunities and challenges for use of tumor spheroids as models to test drug delivery and efficacy. J Control Release. 2012;164(2):192–204. https://doi.org/10.1016/j.jconrel.2012.04.045.
Park H, Go YM, St John PL, Maland MC, Lisanti MP, Abrahamson DR, Jo H. Plasma membrane cholesterol is a key molecule in shear stress-dependent activation of extracellular signal-regulated kinase. J Biol Chem. 1998;273(48):32304–11. https://doi.org/10.1074/jbc.273.48.32304.
Pinho E, Grootveld M, Soares G, Henriques M. Cyclodextrins as encapsulation agents for plant bioactive compounds. Carbohydr Polym. 2014;101:121–35. https://doi.org/10.1016/j.carbpol.2013.08.078.
Ratajczak K, Borska S. Cytotoxic and proapoptotic effects of resveratrol in in vitro studies on selected types of gastrointestinal cancers. Molecules. 2021. https://doi.org/10.3390/molecules26144350.
Rauf A, Imran M, Butt MS, Nadeem M, Peters DG, Mubarak MS. Resveratrol as an anti-cancer agent: a review. Crit Rev Food Sci Nutr. 2018;58(9):1428–47. https://doi.org/10.1080/10408398.2016.1263597.
Sandilya AA, Natarajan U, Priya MH. Molecular view into the cyclodextrin cavity: structure and hydration. ACS Omega. 2020;5(40):25655–67. https://doi.org/10.1021/acsomega.0c02760.
Seo Y, Park J, Choi W, Ju Son D, Sung Kim Y, Kim MK, et al. Antiatherogenic effect of resveratrol attributed to decreased expression of ICAM-1 (intercellular adhesion molecule-1). Arterioscler Thromb Vasc Biol. 2019;39(4):675–84. https://doi.org/10.1161/ATVBAHA.118.312201.
Smoliga JM, Blanchard O. Enhancing the delivery of resveratrol in humans: if low bioavailability is the problem, what is the solution? Molecules. 2014;19(11):17154–72. https://doi.org/10.3390/molecules191117154.
Stella VJ, Rajewski RA. Sulfobutylether-beta-cyclodextrin. Int J Pharm. 2020;583:119396. https://doi.org/10.1016/j.ijpharm.2020.119396.
Tibbitt MW, Anseth KS. Hydrogels as extracellular matrix mimics for 3D cell culture. Biotechnol Bioeng. 2009;103(4):655–63. https://doi.org/10.1002/bit.22361.
Tung YC, Hsiao AY, Allen SG, Torisawa YS, Ho M, Takayama S. High-throughput 3D spheroid culture and drug testing using a 384 hanging drop array. Analyst. 2011;136(3):473–8. https://doi.org/10.1039/c0an00609b.
Varoni EM, Lo Faro AF, Sharifi-Rad J, Iriti M. Anticancer molecular mechanisms of resveratrol. Front Nutr. 2016;3:8. https://doi.org/10.3389/fnut.2016.00008.
Velmurugan BK, Rathinasamy B, Lohanathan BP, Thiyagarajan V, Weng CF. Neuroprotective role of phytochemicals. Molecules. 2018. https://doi.org/10.3390/molecules23102485.
Wu LY, Di Carlo D, Lee LP. Microfluidic self-assembly of tumor spheroids for anticancer drug discovery. Biomed Microdevices. 2008;10(2):197–202. https://doi.org/10.1007/s10544-007-9125-8.
Yang L, Yang L, Tian W, Li J, Liu J, Zhu M, et al. Resveratrol plays dual roles in pancreatic cancer cells. J Cancer Res Clin Oncol. 2014;140(5):749–55. https://doi.org/10.1007/s00432-014-1624-4.
Yasuda H, Marsh HC, Brandt ES, Reilley CN. Preparation of composite reverse osmosis membranes by plasma polymerization of organic compounds. IV. Influence of plasma–polymer (substrate) interaction. J Appl Polym Sci. 1976;20:543–55. https://doi.org/10.1002/app.1976.070200224.
Zhang D, Lv P, Zhou C, Zhao Y, Liao X, Yang B. Cyclodextrin-based delivery systems for cancer treatment. Mater Sci Eng C Mater Biol Appl. 2019;96:872–86. https://doi.org/10.1016/j.msec.2018.11.031.

Publisher's Note